Displacement and Mixed Fibre Beam Elements for Modelling of Slender Reinforced Concrete Structures under Cyclic Loads

Samer Sabry F. Mehanny Gendy [(1)], Ashraf Ayoub [(2)]

[1] Ph.D. Candidate, School of Mathematics, Computer Science & Engineering, Department of Civil Engineering; City, University of London, London, UK; E-mail: Samer.Gendy@city.ac.uk

[2] (corresponding author) Professor, School of Mathematics, Computer Science & Engineering, Department of Civil Engineering; City, University of London, London, UK; E-mail: Ashraf.Ayoub.1@city.ac.uk

Abstract

In this paper, two fibre-based beam elements with enhanced capabilities to consider large displacements and rotations of slender reinforced concrete members are developed. Fibre beam elements were comprehensively used before to model the behaviour of different structural systems with great accuracy. To upsurge the use of the fibre beam elements in modelling complex reinforced concrete (RC) systems such as slender walls and columns, the elements are improved by including the second order effect. Available research from the literature related to large displacements focused mainly on modelling steel and composite members due to the limitations in their material model behaviour. Conversely, the newly developed elements introduced in this paper can precisely model RC members by accounting for their more complex nonlinear material behaviour under reversed cyclic loads. The first element is formulated using a displacement formulation, while the second element is based on a mixed approach that is computationally more complicated but numerically more efficient. Further, the adopted concrete constitutive law accounts for the effect of compression post-peak softening as well as tension stiffening and degradation under cyclic loads. Several correlation studies are presented to highlight the efficiency of the new elements in modelling slender RC structures.

Key words: Large displacement; P-delta; fibre element; slender columns; tension stiffening

Introduction

Fibre beam elements are frequently used to predict the nonlinear response of RC structures under static and dynamic loads. Fibre beam elements use detailed geometry and material models to obtain accurate representation of yielding and inelastic behavior along the length of the member [1-2]. They require less storage capacity and short execution time compared to continuum elements such as membrane and solid elements. Yet, most available RC fibre beam elements do not consider second order effects. Existing second-order fiber-based elements focused mostly on steel and composite structures under monotonic loads [3-6]. Hence, in order to study the actual stability and performance of slender reinforced concrete structures under different loads, second order effects must be considered. The inclusion of second-order effects is necessary to examine slender structures such as long columns, arches, and tall buildings. In such frames, large displacements and rotations are expected to occur and the second-order effect can lead to a higher level of inelastic behaviour that must accounted for in nonlinear analysis.

The calculation of second order forces in numerical algorithms can be carried out using matrix analysis where the geometric stiffness is directly derived from the governing differential equations that consider the second-order effect of the axial force on the flexure response. This offers a simple and accurate method for the consideration of second order effects for beam-column elements. This method is also called the second-order computer program method due to the ease of its implementation in computer routines compared to other conventional methods. The geometric stiffness effect on the forces and displacements of the member usually varies between 10 to 25% depending on the ratio between the lateral and axial loads [7].

Two types of deformations are associated with the second order analysis. First, the P-δ, (called the small P-delta), where δ is related to the local deformation with respect to the chord

of the element end nodes and can be considered by subdividing the element into smaller segments. Second, the P-Δ, (called the big P-delta), where Δ is related to member end displacements and should be considered in the numerical formulation to accurately model the second order structural response.

In a previous study [8], the authors formulated a displacement-based beam element for large deformations of plastic plane frames. The effect of axial force was included in small deflection theories; and the element was formulated in a body-attached coordinate to separate between rigid body and deformational rotations.

Another study presented a two-dimensional displacement-based and generalized mixed variational finite element that can be used to model arbitrary large displacements and rotations with small strains [9]. The research in [4] aimed to develop a three-dimensional force-based fibre beam element that considers inelastic large displacements. The algorithm is as a generalization of the state determination procedure presented in [10] for linear geometry/nonlinear material analysis, and the procedure described in [3] for linear material/nonlinear geometry. However, the element was only used to investigate the performance of steel frames under static monotonic loads. The element state determination was implemented in the software packages FedeasLab and OpenSees.

The authors in [5] presented several beam column finite element formulations for full nonlinear distributed plasticity analysis of two-dimensional steel frame structures. For the displacement-based and the mixed elements, the second order effect was included in the corotational formulation. Another research work in [11] promoted a numerical model for non-linear large-displacement dynamic analysis of steel beam-columns. The model was utilized to investigate the behaviour of beam-column steel elements subjected to blast loading. The steel members were restrained at their ends by rotational and translational springs producing second order effects. Further, the study in [6] developed a 3D distributed

plasticity beam element using mixed formulations for composite circular concrete-filled steel tubes. The formulation considered large displacements and rotations using a corotational frame transformation.

Recently, a new study used a large displacement corotational formulation to analyse planar functionally graded sandwich beams [12]. The beams were composed of a metallic steel core and two top and bottom ceramic faces. The study highlighted the importance of considering the effect of plastic deformation in large displacement analysis.

In this paper, two planar fibre beam elements are presented for the analysis of slender RC members under cyclic loads. The first one uses a displacement-based technique to calculate the stiffness and the resisting forces of members. In this method, the equilibrium is satisfied in a weighted integral sense. For this technique, the use of a fine mesh is essential in plastic zones in order to represent precisely the curvature and strain distributions. The second element uses a mixed-based technique, where both displacements and internal forces are interpolated independently and the equilibrium is satisfied in a section by section basis. The mixed method requires less number of finite elements to simulate structural responses; however its state determination algorithm is much more complex.

The proposed elements are based on the work by [13] and [5]; to incorporate second order effects into displacement and mixed-based elements. Unlike the element of [5], which was used to analyse simple steel members under static monotonic loads only, the proposed elements developed herein are able to model the complex behaviour of normal and high-performance reinforced concrete as well as steel members under both monotonic, and severe cyclic loads. They can also monitor the behaviour of the structure at the element, section and fibre level. Further, the state determination process of the elements is modified for improved numerical efficiency.

The newly developed elements will be used to analyse RC members under different static and dynamic loading conditions. They take into account the geometric nonlinearity and benefit from sophisticated material models that can accurately simulate the nonlinear behaviour of concrete and steel materials, which will help in studying local effects in details. The elements are implemented in the research-oriented finite element analysis program FEAP developed by Taylor [14].

Transformation between Corotational and Global Systems

The two elements formulated in this chapter follow Navier's three principles of mechanics: The stress equilibrium, the strain compatibility and the constitutive relationships of steel and concrete. First the two elements are formulated in a corotational system where rigid body modes are removed and small strains but large displacements are assumed. For the present formulation, the axial force is constant and does not change along the element, while distributed loads are not considered in the current fibre beam element formulation. Only internal loads on the members are lumped at nodal points along the members, and are transformed to the end loaded members.

The matrix T_r links the element nodal forces in the global system with the element internal forces in the corotational system [5]:

$$\bar{Q} = {T_r}^T Q \tag{1}$$

$$T_r = \begin{bmatrix} -\frac{\sin\beta}{L} & \frac{\cos\beta}{L} & 1 & \frac{\sin\beta}{L} & -\frac{\cos\beta}{L} & 0 \\ -\frac{\sin\beta}{L} & \frac{\cos\beta}{L} & 0 & \frac{\sin\beta}{L} & -\frac{\cos\beta}{L} & 1 \\ -\cos\beta & -\sin\beta & 0 & \cos\beta & \sin\beta & 0 \end{bmatrix} \tag{2}$$

Where $\bar{Q}$ and Q are the nodal forces in the global and corotational systems respectively, and are shown in Figure (1), and β is the final angle of the deformed beam element:

$$\beta = \arctan\left(\frac{(y_2+v_2)-(y_1+v_1)}{(x_2+u_2)-(x_1+u_1)}\right) \quad (3)$$

where u is the end displacement in the horizontal direction and v is the end displacement in the vertical direction. Subscripts *1* and *2* refer to the element ends respectively.

In addition, the transformation matrix T_r is also used for the transformation of the displacements between the corotational and global system:

$$\delta\bar{q} = {T_r}^T \delta q \quad (4)$$

Where $\bar{q}$ and q are the element end displacements in the global and corotational systems respectively.

Similarly, the stiffness matrix is transformed between the two systems using the same mapping matrix. However, an additional term K_G that includes the effects of element internal forces on the element stiffness must be included:

$$K_{elem(global)} = {T_r}^T K_{elem}\, T_r + K_G \quad (5)$$

Where K_G is the well-established external geometric stiffness matrix.

Formulation of the Displacement-Based Element

In the classical displacement-based method, the equilibrium is achieved only in a weighted integral sense. The displacements serve as primary variables and the principle of virtual displacements is implemented to obtain the solution.

The Green–Lagrange strain of the element reference axis in the natural frame that is derived from the displacement field can be defined as:

$$\hat{\varepsilon} = \frac{du}{dx} + \frac{1}{2}\left(\frac{dv}{dx}\right)^2 + \frac{1}{2}\left(\frac{du}{dx}\right)^2 \quad (6)$$

Where the transverse and axial displacements v and u are represented,respectively, by cubic and linear functions along the element length:

$$v = \begin{bmatrix} 0 & x - \frac{2x^2}{L} + \frac{x^3}{L^2} & -\frac{x^2}{L} + \frac{x^3}{L^2} \end{bmatrix} q = N_V^T q \tag{7}$$

$$u = [x/L \quad 0 \quad 0]\, q = N_U^T q \tag{8}$$

The third term in equation (6) is neglected since the axial deformation of the element chord within the natural system is relatively small. And thus the strain increment is represented by:

$$\Delta\hat{\varepsilon} = \left(N'^T_U + \frac{1}{2} q^T N'_V N'^T_V \right) \Delta q \tag{9}$$

and similarly for the curvature:

$$\Delta\hat{K} = \left(N''^T_V \right) \Delta q \tag{10}$$

So the increment in the generalized strains can be stated as:

$$\Delta\hat{d} = \begin{Bmatrix} \Delta\hat{\varepsilon} \\ \Delta\hat{K} \end{Bmatrix} = N_\Delta \, \Delta q \tag{11}$$

Where the interpolation function N_Δ accounts for P-Δ effects, and can be expressed as:

$$N_\Delta = \begin{bmatrix} \frac{1}{L} & \left(1 - \frac{4x}{L} + \frac{3x^2}{L^2}\right)^2 q_2 + \left(1 - \frac{4x}{L} + \frac{3x^2}{L^2}\right)\left(-\frac{2x}{L} + \frac{3x^2}{L^2}\right) q_3 & \left(1 - \frac{4x}{L} + \frac{3x^2}{L^2}\right)\left(-\frac{2x}{L} + \frac{3x^2}{L^2}\right) q_2 + \left(\frac{2x}{L} + \frac{3x^2}{L^2}\right)^2 q_3 \\ 0 & -\frac{4}{L} + \frac{6x}{L^2} & -\frac{2}{L} + \frac{6x}{L^2} \end{bmatrix} \tag{12}$$

The increment in the generalized strains (curvature and axial strain) at any section can be assembled in a vector form as follows:

$$\Delta\hat{d} = N_1 \Delta q + \begin{Bmatrix} 0 \\ 1 \end{Bmatrix} \Delta q^T N_2 q^i + \frac{1}{2} \begin{Bmatrix} 0 \\ 1 \end{Bmatrix} \Delta q^T N_2 \Delta q \tag{13}$$

Where Δq is the increment between the current Newton-Raphson step *i* and the previous step *i-1*; while q^i is the total value of the displacement at the current step. Consequently:

$$N_1 = \begin{bmatrix} \frac{1}{L} & 0 & 0 \\ 0 & \frac{-4}{L} + \frac{6x}{L^2} & \frac{-2}{L} + \frac{6x}{L^2} \end{bmatrix} \tag{14}$$

$$N_2 = \begin{bmatrix} 0 & 0 & 0 \\ 0 & \left(1 - \frac{4x}{L} + \frac{3x^2}{L^2}\right)^2 & \left(1 - \frac{4x}{L} + \frac{3x^2}{L^2}\right)\left(\frac{-2x}{L} + \frac{3x^2}{L^2}\right) \\ 0 & \left(1 - \frac{4x}{L} + \frac{3x^2}{L^2}\right)\left(\frac{-2x}{L} + \frac{3x^2}{L^2}\right) & \left(-\frac{2x}{L} + \frac{3x^2}{L^2}\right)^2 \end{bmatrix} \tag{15}$$

N_1 and N_2 are the final shape functions representing first-order and second-order effects respectively. It can be noted that the second and third terms of equation (13) contain the P-delta higher order terms.

To avoid membrane locking effects [15], the second and third terms of the generalized strain equation are averaged along the element length. Therefore, equation (13) becomes:

$$\Delta\hat{d} = N_1 \Delta q + \begin{Bmatrix} 0 \\ 1 \end{Bmatrix} \frac{1}{L} \int_0^{L_0} \Delta q^T N_2 q^i + \frac{1}{2} \begin{Bmatrix} 0 \\ 1 \end{Bmatrix} \frac{1}{L} \int_0^{L_0} \Delta q^T N_2 \Delta q \tag{16}$$

In the displacement formulation, the equilibrium equation is satisfied in a weak form. Accordingly, and with the substitution of the derived shape functions:

$$\delta q^T \int_0^{L_0} N_\Delta^T (K_{sec}^{i-1} \Delta d^i + F_{sec}^{i-1})\, dx = 0 \tag{17}$$

Where δq is a weighting function, K_{sec}^{i-1} is the section stiffness matrix at the previous Newton-Raphson iteration *i-1*, and F_{sec}^{i-1} is the corresponding section resisting force vector and is defined as $\begin{Bmatrix} P \\ M \end{Bmatrix}$; P is the section axial force and M is the section bending moment.

Finally, the previous equation is used to calculate the element stiffness matrix and the resisting load vector accounting for the second order effects [16]. Consequently, the element stiffness matrix is:

$$\boldsymbol{K} = \left(K_g + \int_0^{L_0} N_\Delta^T\, K_{sec}\, N_\Delta dx\right) \tag{18}$$

Where K_g is the internal geometric stiffness matrix and is equal to:

$$K_g = Q_1 \begin{bmatrix} \frac{2L}{15} & \frac{-L}{30} & 0 \\ \frac{-L}{30} & \frac{2L}{15} & 0 \\ 0 & 0 & 0 \end{bmatrix} \tag{19}$$

and the element resisting load vector is:

$$F_{elem} = \int_0^{L_0} {N_\Delta}^T \, F_{sec} \, dx \tag{20}$$

Formulation of the Mixed-Base Element

In the mixed formulation, displacement fields and stress resultant forces are both interpolated individually along the length of the element [13, 5]. Linear and cubic interpolation functions are selected for the transverse (v) and axial(u) deformations respectively, so N_u and N_v are the same as in the displacement-based formulation (Equations 7 -8).

For the stress-resultant force fields, the shape functions are constructed from a constant axial force field and a linear moment field, resulting in:

$$F_{sec} = N_F Q \; ; \tag{21}$$

$$N_F = \begin{bmatrix} 1 & 0 & 0 \\ 0 & \frac{x}{L} - 1 & \frac{x}{L} \end{bmatrix} \tag{22}$$

Where N_F is the force shape function.

The compatibility is imposed in a weak form by multiplying the weighting function with the difference of the strains calculated from the displacement shape function $\hat{d}$ at the current step, and the strains calculated from the inverse of the force-deformation relation; then integrating along the element length:

$$\int_0^{L_0} \delta {F_{sec}}^T \left(\hat{d}^i - (f_{sec}^{i-1} \Delta F_{sec}^i + d^{i-1}) \right) dx = 0 \tag{23}$$

Where f_{sec}^{i-1} is the section flexibility matrix at the previous step, and is equal to the inverse of the section stiffness matrix.

Substituting the displacement and force interpolation functions result in:

$$G\Delta q^i - f_{elem}^{i-1}\Delta Q^i - q_r^{i-1} = 0 \tag{24}$$

Where:

$f_{elem}^{i-1} = \int_0^{L_0} N_F^T \, f_{sec}^{i-1} \, N_F dx$ is the element flexibility matrix (25)

$$G = \int_0^{L_0} N_F^T \;\; N_\Delta dx \tag{26}$$

G is the integration of the product of the displacement and force shape functions along the element length. It contains higher order terms to include the second order effects:

$$G = \begin{bmatrix} 1 & \frac{2Lq_2}{15} - \frac{Lq_3}{30} & -\frac{Lq_2}{30} + \frac{2Lq_3}{15} \\ 0 & 1 & 0 \\ 0 & 0 & 1 \end{bmatrix} \tag{27}$$

and $q_r^{i-1} = \int_0^{L_0} N_F^T d^{i-1} \, dx - Gq^{i-1}$ (28)

$q_r^{i-1}$is the element residual deformation vector which represents the compatibility error between the nodal displacements and deformation fields.

The weighted integral of the compatibility equation (23) is coupled with the weighted integral of the equilibrium equation (17) to evaluate the element stiffness matrix and resisting load vector, resulting in (29):

$$K_{elem}\,\Delta q = F_{ext} - F_{elem} \tag{29}$$

Where:

$$K_{elem} = \left(K_g + \int_0^{L0} G^T \, f_{elem}^{-1} \, G \, dx\right) \tag{30}$$

$$F_{elem} = G^T F_{elem} + G^T f_{elem}^{-1} \; q_r^{i-1} \quad (31)$$

and F_{ext} is the vector of external loads.

The element state determination follows the procedure described in details in [13] and requires an internal element iteration in addition to the global Newton-Raphson iteration. At convergence of the internal iteration, the element residual deformation q_r^{i-1} vanishes.

Material Models

The advantage of this fibre beam element is that it combines the displacement and mixed based formulations that consider second order effects with advanced nonlinear material models that permit the accurate simulation of the behaviour of reinforced concrete members.

The new elements use the modified Kent and Park [17] stress strain model for the concrete material, which is shown in Figure (2). The cyclic model takes into account the concrete damage and hysteresis, while retaining computational efficiency.

The present concrete material model recognises the ability of concrete to carry tension and identifies the tension stiffening effect, which is known as the capability of cracked concrete to carry tensile stresses and to participate in the stiffness of the member. As the cracks increase, this participation diminishes and the tension stiffening decreases progressively. Therefore, the concrete stress-strain relation simulates this behaviour by reducing the tensile stress, after reaching the tensile strength, until it reaches a zero value. The reduction of tensile stress can follow a linear, multilinear or exponential path.

For the steel material model, the Menegotto-Pinto cyclic stress-strain curve of mild steel bar is used as shown in Figure (3). The model accounts for the Bauschinger effect under cyclic loads. The reinforcing steel model adopted with the current fibre beam element is the one

presented in [18], which modified the stress-strain relationship of steel originally developed in [19] to consider isotropic hardening.

The fibrous materials are modelled by controlling the values of the concrete tensile strength and tension softening stiffness. Three cases are accounted for as shown in Figure (4):

Case 1: simulates the presence of a high percentage of fibres; in this case the tensile strength f_t is typically chosen more than 10% of the compression strength and the tension softening stiffness slope is chosen as close to zero to model an ideal constant tensile strength.

Case 2: simulates the presence of a moderate percentage of fibres; in this case the tensile strength is chosen less than 10% of the compression strength and the tension softening stiffness value E_{ts} is chosen as a linear moderate decreasing line (e.g. $E_{ts} = 1000$ MPa).

Case 3: simulates the absence of fibres leading to an infinite slope to simulate a brittle tension failure (e.g. $E_{ts} = 10^6$).

Validation of the Finite Element Model

The recently developed models are validated by comparing their results with several benchmark experiments. All the chosen specimens undergo large deformations due to the slenderness of the section. I addition, fibrous materials were added to the concrete mix of several specimens and their effect was noted on the behaviour. As will be seen, the models were able to accurately imitate the performance of the RC sections under monotonic and cyclic loading, which emphasizes the accuracy and efficacy of the newly developed elements.

Barrera et al. Experiment

The first experiment that will be used for the validation of the new elements for reinforced concrete structures is a test performed in [20] by Barrera et al. to examine forty-four rectangular slender reinforced concrete columns with different sections, under combined

axial load and lateral force. The use of high strength concrete (HSC) in the column produced smaller cross sections which increased its slenderness and resulted in a major second order effect. A constant axial load and a monotonic lateral force were applied up to failure of the columns. The test setup is displayed in Figure (5), and the geometry and dimensions of the specimens are shown in Figure (6). After testing, two simplified methods from Eurocode 2 and ACI-318 were used by the authors for comparison with the experimental results, and were both found very conservative.

The developed elements are used to compare the results of specimen (H60-10.5-C0-2-30). This sample has a cross section of 200x150 mm and a nominal concrete strength of 60.5 MPa, steel young's modulus of 200 GPa, longitudinal steel yielding stress of 537 MPa and longitudinal reinforcement of 6Ø10 bars. A constant axial force that equals 432 kN was applied to the specimen. The fibre beam model was constructed using only 4 elements. This was sufficient to reach convergence for both the displacement and the mixed elements. Further, every element was divided internally into 5 sections and the sections were divided into 10 concrete fibres and 6 steel fibres that represent the column reinforcement (Figure (7)).

The concrete material parameters were assigned the following values:

$f'_c = 60.5$ MPa, $\varepsilon_c = 0.002$, $\varepsilon_u = 0.09$, $\lambda = 0.01$, $f_t = 3.0$ MPa and $E_{ts} = 10^6$ MPa.

Where:

f'_c: concrete compressive strength

ε_c: concrete strain at maximum strength

ε_u: concrete strain at crushing strength

$\lambda = \frac{E_c}{E_u}$ (E_c and E_u are defined in Figure (2)).

f_t: $concrete$ tensile strength

E_{ts}: tension softening stiffness (absolute value)

The steel material parameters were assigned the following values:

$f_y = 537.0$ MPa, $E_0 = 200000$ MPa, $b = 0.01$, $a_1 = 0.01$, $a_2 = 20.0$ MPa , $a_3 = 18.5$ MPa and $a_4 = 0.1$

Where:

f_y: steel yield strength

E_0: steel Young's modulus

b: strain hardening ratio

$a_1 , a_2, a_3 \; and \; a_4$: isotropic hardening parameters described in [18-19]

Figure (8) shows the load displacement curve of the tested column. It is clear that both fibre beam elements were able to follow the output path of the experiment until failure. The previous displacement-based element that did not consider the second order analysis strongly missed the path and produced an error up to double the load value near failure. It is noticeable that the higher the load, the more the second order effect increases.

Using the mixed element, Figure (9) presents the full vertical displacement distribution along the element length under four different lateral force values. These deformed shapes are very similar to the ones retrieved from the experiment. As an example, the experimental deformed shape at a lateral force of 16.56 KN, which is plotted in Figure (9) matches well with the analytical results using the mixed element.

In Figure (10), a comparison is presented between the curvatures at the maximum load level for the displacement and mixed elements with the second order effect. It is clear that while the mixed element still produces a smooth curve, the displacement element requires more divisions to match with the mixed element's results. The output curve of the displacement-based element with higher element divisions (12 elements) approaches the one of the mixed element (4 divisions); however, the produced curve was still not sufficiently

smooth and accurate. Consequently, the higher accuracy of the mixed element in the determination of the curvature in the case of inelastic deformations is apparent.

Moreover, the moment-curvature plot for the section at midspan (section 5 of element 2) is shown in Figure (11). It is clear that the second order analysis produced a weaker behavior. it can be seen from the graph that the higher the curvature, the larger the second order effect. However, since the section behavior is only affected by Green-Lagrange small strains, second order effects are still not significant. It is clear that the second order analysis, at the section level, produced moments reduced by up to 9% than those without second order analysis. The major influence of second order effects are observed at the global level due to the effect of large displacements and rotations.

Caballero-Morrison et al. Experiment

Later, another experimental study in [21] used the same previous type of specimens, which represent two columns of two connected floors joined by a stub, to test steel fibre-reinforced high strength concrete (SFRC) slender columns, but this time under cyclic loading. HSC was used for the slender columns to increase its deformation capacity. Two samples were selected to be modelled using the fibre beam elements. The detailed geometries of the specimens are the same as the ones used in the previous experiment. The first sample (NF00L05V2S100) is a normal strength concrete, with f'_c= 33.57 MPa, a cross section of 260x150 mm and longitudinal reinforcement of 6Ø12. No steel fibres were added to this sample. The second specimen (HF60L05V1S50) is a HSC, with f'_c= 81.10 MPa, a cross section of 260x150 mm with longitudinal reinforcement of 6Ø12 and with steel fibre content of 60 kg/m^3 (equivalent to a volumetric ratio of 0.76%). The fibre content was modelled by assigning the element a negligible post-peak tension softening stiffness.

The concrete material parameters were assigned the following values:

For specimen (NF00L05V2S100):

$f'_c = 33.57$ MPa, $\varepsilon_c = 0.002$, $\varepsilon_u = 0.12$, $\lambda = 0.01$, $f_t = 0.1$ MPa and $E_{ts} = 10^6$ MPa.

For specimen (HF60L05V1S50):

$f'_c = 81.1$ MPa, $\varepsilon_c = 0.0027$, $\varepsilon_u = 0.20$, $\lambda = 0.01$, $f_t = 8.0$ MPa and $E_{ts} = 1000.0$ MPa.

The steel material parameters were assigned the following values:

For specimens (NF00L05V2S100) and (HF60L05V1S50):

$f_y = 548.0$ MPa, $E_0 = 200000$ MPa, $b = 0.02$, $a_1 = 0.01$, $a_2 = 20.0$ MPa , $a_3 = 18.5$ MPa and $a_4 = 0.1$

The test procedure consisted of first applying a constant compression horizontal load corresponding to the relative normal force, followed by the cyclic lateral load. The same finite element model described in the first experiment was used. Figure (12) shows the fibre beam element cross section mesh used for the two specimens.

A sensitivity study was performed for the two models and it was found that the displacement-based model requires to be constructed with 14 elements to reach convergence and to capture the external retraction hysteric path; whereas the mixed-based model required only 4 elements to achieve full convergence. Five sections are typically adopted in the model since this discretization can accurately represent the plastic hinge zone in concrete structures and ten concrete fibres per section are typically selected [1].

In Figure (13), the results of the two fibre beam models are compared with the experimental data of specimen (NF00L05V2S100). It is clear that they were both able to model the behaviour to a very good extend. In Figure (14), the elements were compared with the experimental results of sample (HF60L05V1S50); also good matching can be seen in the output graph. Further, when second order effects are not considered, a higher load path is depicted, as shown in Figure (14).

From the plot in Figure (14), the influence of using HSC and adding fibrous materials can be distinguished with respect to the deformation that the sample has undergone and the shape of the hysteric curves. Therefore, this example establishes the ability of the enhanced elements to model slender reinforced concrete members subjected to cyclic loading while accounting for the presence of steel fibres in the concrete mix.

Figure (15) shows the cyclic stress-strain curve of the bottom steel rebar at the midspan section of sample HF60L05V1S50. In this case, second order effects produced higher strain values that pushed the bar deep into the inelastic range further amplifying its nonlinear response.

Dundar et al. Experiment

The fibre beam elements are finally used to model the experimentally-tested specimens of Dundar et al. [22], where slender reinforced concrete columns strengthened with steel fibres and carbon fibre polymer sheets were tested under combined axial load and bending in order to determine their behaviour.

The tested columns had a length of 1300 mm, a cross section of 125x125 mm along with two heavily reinforced concrete brackets with dimensions of 200x200x200 mm, that were installed at the columns ends to allow for the application of loads. The columns had a slenderness ratio of 34.67. Figure (16) shows the experiment setup.

For all tested columns, the longitudinal reinforcement was Ø8 at each corner of the section and the lateral reinforcement was Ø6 with spacing 100 mm. The yield strength of the longitudinal reinforcement was 550 MPa. The columns were loaded with pinned-end conditions and lateral deformations of the specimens were recorded at the column mid height.

Two specimens were chosen to be modelled with the fibre beam elements. Specimen (C2-II) with a concrete strength of 61.91 MPa and specimen (C2-II-SF) with a concrete

strength of 53.13 MPa and containing 60 kg/m^3 steel fibre in the concrete mix. Both specimens had two layers of carbon fibre reinforced polymer (CFRP).

The concrete material parameters were assigned the following values:

For specimen (C2-II):

$f'_c = 61.91$ MPa, $\varepsilon_c = 0.002$, $\varepsilon_u = 0.12$, $\lambda = 0.01$, $f_t = 0.1$ MPa and $E_{ts} = 10^6$ MPa.

For specimen (C2-II-SF):

$f'_c = 53.13$ MPa, $\varepsilon_c = 0.002$, $\varepsilon_u = 0.12$, $\lambda = 0.01$, $f_t = 5.0$ MPa and $E_{ts} = 0.001$ MPa.

The steel material parameters were assigned the following values:

For specimens (C2-II) and (C2-II-SF):

$f_y = 550.0$ MPa, $E_0 = 210000$ MPa, $b = 0.02$, $a_1 = 0.01$, $a_2 = 20.0$ MPa , $a_3 = 18.5$ MPa and $a_4 = 0.1$

The two samples were subjected to an eccentricity of 50 mm around the two horizontal axis. Every column was divided into a number of elements and each element was divided internally into 5 sections. Two different types of cross sections were defined in the finite element models. The first one (125x125 mm), for the intermediate cross section, and was divided into 10 concrete fibres and 4 steel fibres; and the second one (200x200 mm), was assigned to the column ends, and was divided into 10 concrete fibres and 9 steel fibres as shown in Figures (17 & 18).

The presence of the CFRP sheets affect the ductility and confinement of the columns and was taken into account in the finite element model by assigning a higher compression post-peak stiffness value for the concrete material model resulting in a strain of 0.04 at a stress value of 20% of the concrete strength. Further, the addition of steel fibres was accounted for by assigning a negligible tension softening stiffness. The column was divided into only 4 members for the mixed element per half span (the minimum possible number of division as

two different sections are assigned) and 12 members for the displacement-based element. The two fibre beam elements with the second order effect were able to model the two slender columns accurately and to follow the load displacement path for both (C2-II) & (C2-II-SF) as shown in Figures (19-20). From the plots, it can be seen that disregarding the second order effect gives an exaggerated path for the load-displacement curves. In addition, the plots reveals that both elements can recognise and simulate the presence of the fibrous material while taking into account the second order effect.

Further, the mixed element with four divisions is then used to generate the vertical displacement along the length of the column (Figure 21) and moment distribution at the axial load axis (Figure 22). The results were selected at the case of maximum load (258 KN), where the middle of the column was subjected to the highest displacement of about 8.5 mm. The model was able to predict the maximum bending moment rather accurately, with a value of 2.4 KN.m.

Conclusion

Two robust finite element models based on a fibre beam element formulation were presented. The elements consider second order effects and can simulate the nonlinear behaviour of reinforced concrete members with great accuracy. The first element is formulated using a displacement-based method while the second adopts a mixed approach. It was found that the displacement element requires more division to reach convergence; on the other hand, the mixed model requires fewer elements per member. Correlation studies with experimentally-tested slender reinforced concrete specimens proved the elements can simulate the complex local and global nonlinear response of the members rather accurately, including the effect of fibrous materials in the concrete mix. The new elements can therefore be effectively used in modelling slender reinforced concrete structures such as tall columns and walls.

References

[1] Spacone, E., Filippou, F. and Taucer, F. (1996). Fibre beam-column model for non-linear analysis of R/C frames: Part I. formulation. Earthquake Engineering & Structural Dynamics, 25(7), pp.711-725.

[2] Mullapudi, T. and Ayoub, A. (2010). Modeling of the seismic behavior of shear-critical reinforced concrete columns. Engineering Structures, 32(11), pp.3601-3615.

[3] Neuenhofer, A. and Filippou, F. (1998). "Geometrically nonlinear flexibility-based frame finite element." Journal of Structural Engineering, 124(6), 704–711.

[4] De Souza, R. (2000). Force-based Finite Element for Large Displacement Inelastic Analysis of Frames. Doctor of Philosophy. University of California, Berkeley.

[5] Alemdar, B. and White, D. (2005). "Displacement, flexibility, and mixed beam–column finite element formulations for distributed plasticity analysis." Journal of structural engineering, 131(12), 1811–1819.

[6] Denavit, M. and Hajjar, J. (2012). Nonlinear Seismic Analysis of Circular Concrete-Filled Steel Tube Members and Frames. Journal of Structural Engineering, 138(9), pp.1089-1098.

[7] Wilson, E. (1998). Three dimensional static and dynamic analysis of structures. Berkeley, Calif.: Computers and Structures Inc.

[8] Hsiao, K.M., Hou, F.Y., and Spiliopoulos, K. (1988). Large displacement analysis of elasto-plastic frames. Computers & Structures, 28(5), pp.627-633.

[9] Nukala, P. K. 1997. "Three-dimensional second-order inelastic analysis of steel frames." PhD thesis, Purdue Univ., West Lafayette, Ind.

[10] Neuenhofer, A. and Filippou, F. (1997). "Evaluation of nonlinear frame finite-element models." Journal of Structural Engineering, 123(7), 958–966.

[11] Heidarpour, A. and Bradford, M. (2011). Beam–column element for non-linear dynamic analysis of steel members subjected to blast loading. Engineering Structures, 33(4), pp.1259-1266.

[12] Nguyen, D. and Tran, T. (2016). A Corotational Formulation for Large Displacement Analysis of Functionally Graded Sandwich Beam and Frame Structures. Mathematical Problems in Engineering, 2016, pp.1-12.

[13] Ayoub, A. and Filippou, F. (2000). Mixed Formulation of Nonlinear Steel-Concrete Composite Beam Element. Journal of Structural Engineering, 126(3), pp.371-381.

[14] Taylor, R. (2014). FEAP - Finite Element Analysis Program. Berkeley: University of California.

[15] Crisfield, M. A. (1991). Nonlinear finite element analysis of solids and structures, Vol. 1, Wiley, New York.

[16] Mullapudi, T.R., and Ayoub, A.S. (2013). Nonlinear Analysis of Reinforced Concrete Walls under Three-Dimensional Loading. Magazine of Concrete Research, 65(3): 172-184.

[17] Scott, B., Park, R. and Priestley, M. (1982). Stress-Strain Behavior of Concrete Confined by Overlapping Hoops at Low and High Strain Rates. ACI Journal Proceedings, 79(1), pp.13-27.

[18] Filippou, F., Popov, E. and Bertero, V. (1983). Effects of bond deterioration on hysteretic behavior of reinforced concrete joints. Earthquake Engineering Research Center, Report No. UCB/EERC-83/19. Division of Structural Engineering and Structural Mechanics, University of California, Berkeley, p.191.

[19] Menegotto, M. and Pinto, P. (1973). Method of Analysis for Cyclically Loaded Reinforced Concrete Plane Frames Including Changes in Geometry and Nonelastic Behavior of Elements under Combined Normal Force and Bending. In: IABSE symposium on resistance and ultimate deformability of structures acted on by well-defined repeated loads. Final Report, Lisbon, pp.15-22.

[20] Barrera, A., Bonet, J., Romero, M. and Miguel, P. (2011). Experimental tests of slender reinforced concrete columns under combined axial load and lateral force. Engineering Structures, 33(12), pp.3676-3689.

[21] Caballero-Morrison, K., Bonet, J., Navarro-Gregori, J. and Serna-Ros, P. (2013). An experimental study of steel fiber-reinforced high-strength concrete slender columns under cyclic loading. Engineering Structures, 57, pp.565-577.

[22] Dundar, C., Erturkmen, D. and Tokgoz, S. (2015). Studies on carbon fiber polymer confined slender plain and steel fiber reinforced concrete columns. Engineering Structures, 102, pp.31-39.

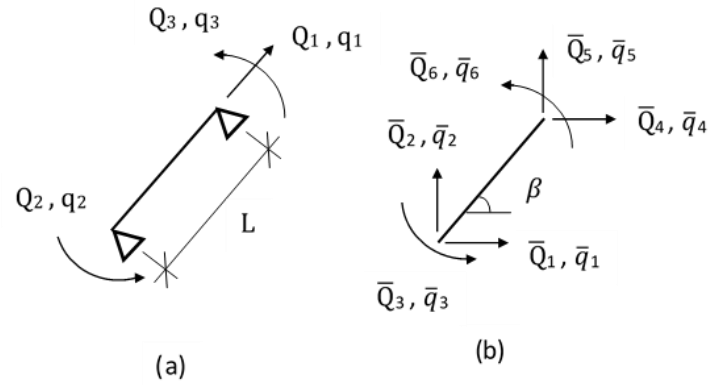

Figure (1): Element forces and displacement degrees of freedom in: (a) corotational and (b) global system

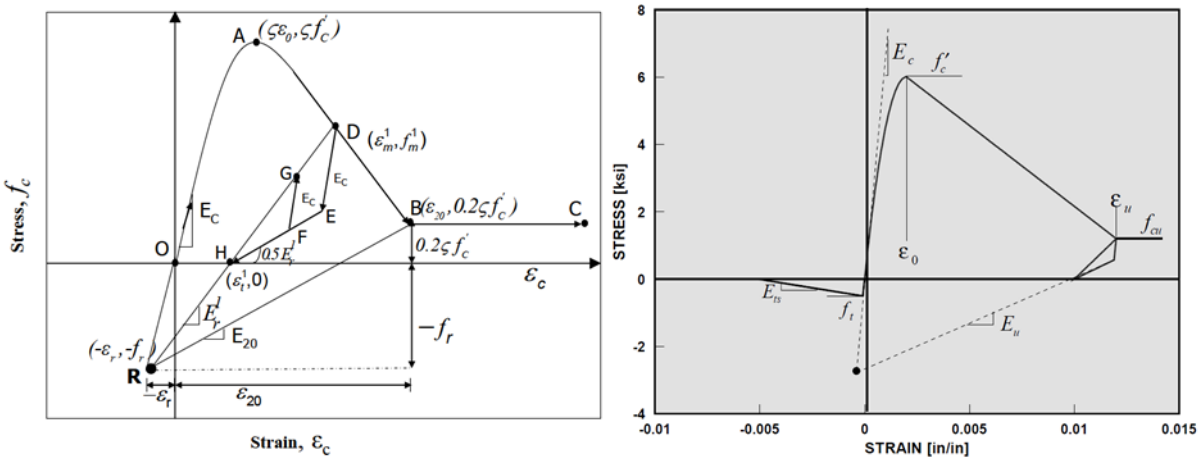

Figure (2): Stress-strain curve of softened Concrete (a) Cyclic (b) Material parameters of Monotonic envelopes of concrete model

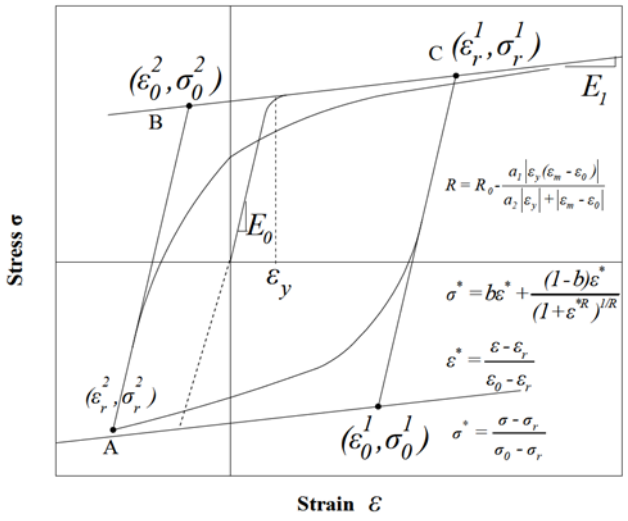

Figure (3): Menegotto-Pinto Cyclic stress-strain curve of mild steel bar

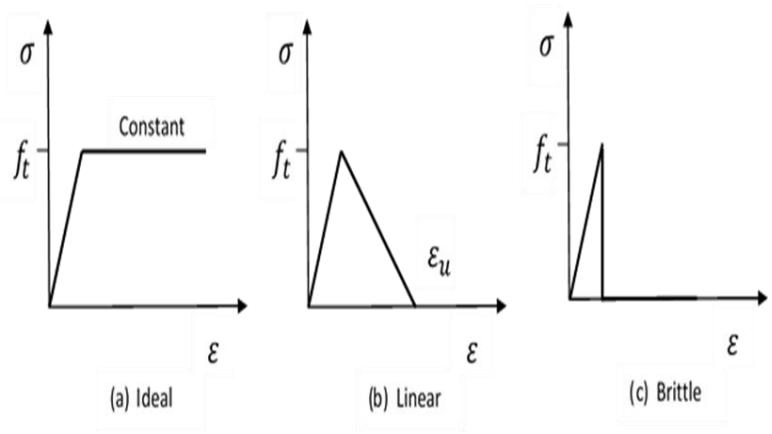

Figure (4): Different tension softening stiffness

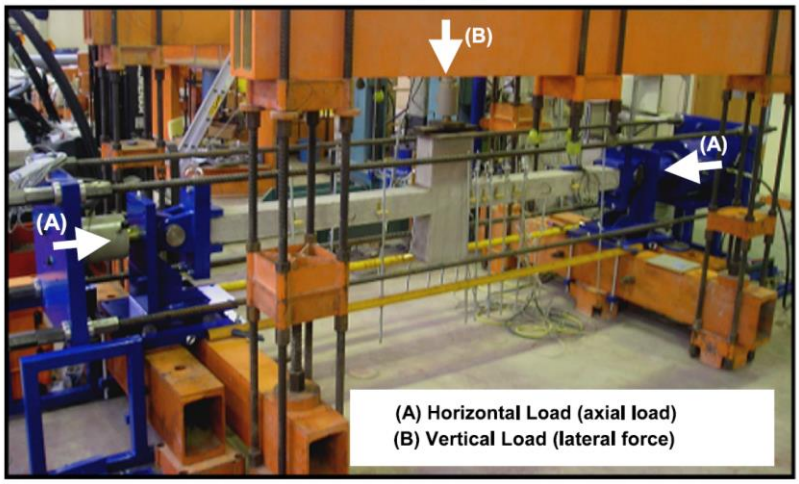

Figure (5): Test framework of Barrera et al. Specimen [20]

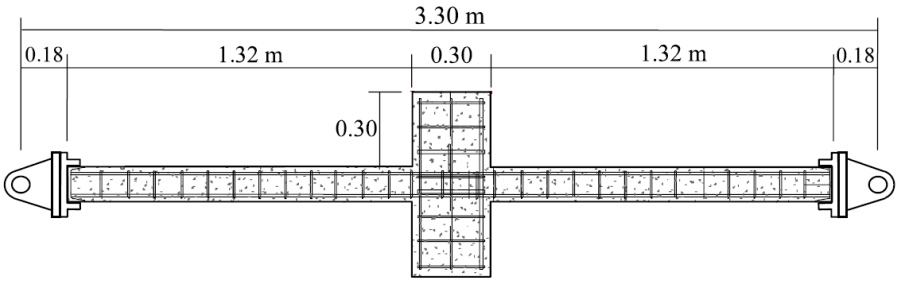

Figure (6): Geometry and dimensions of Barrera et al. Specimen [20]

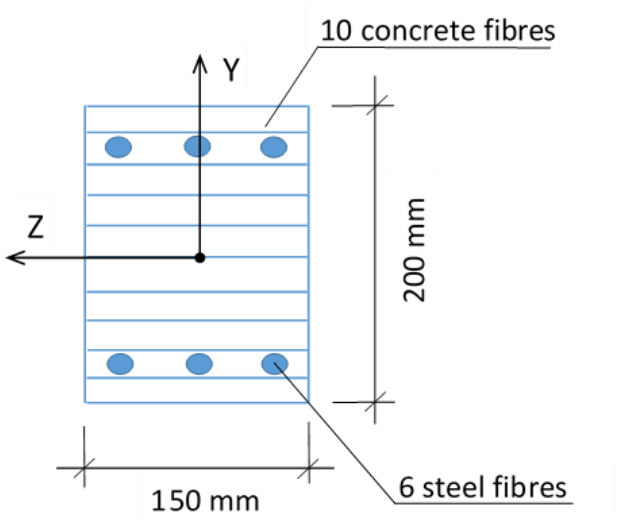

Figure (7): Fibre beam element cross section mesh for specimen H60-10.5-C0-2-30

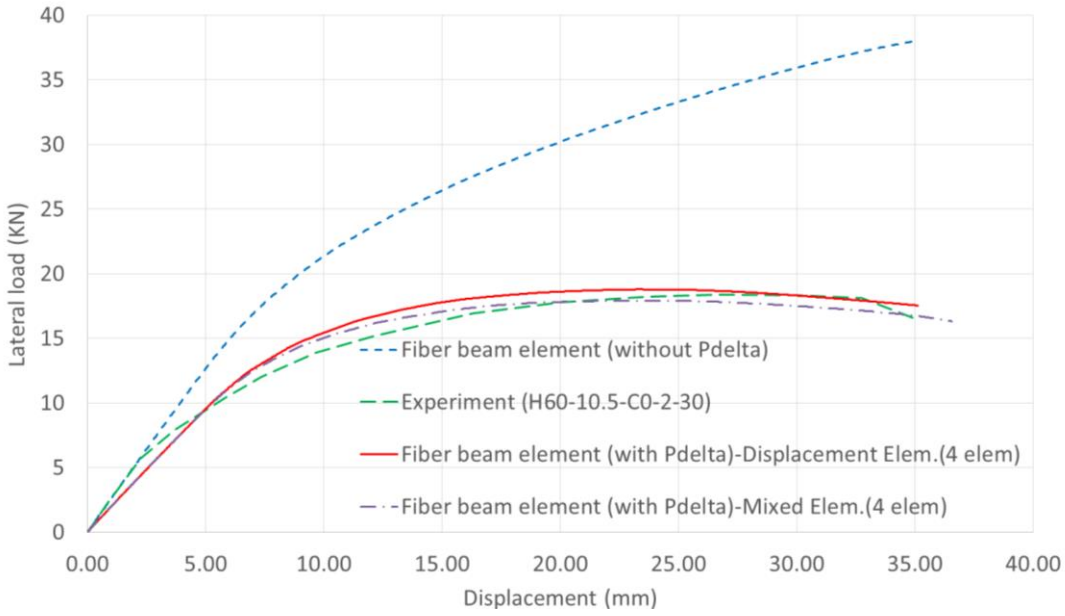

Figure (8): Analytical and Experimental Load displacement curve for column H60-10.5-C0-2-30

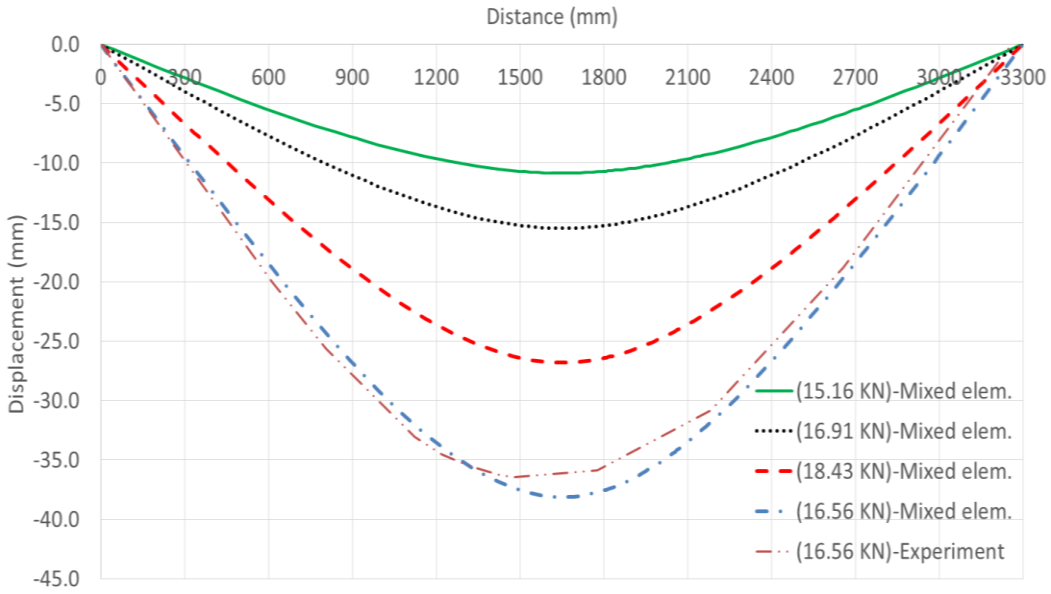

Figure (9): Vertical Displacements along the column H60-10.5-C0-2-30 under different Lateral Forces

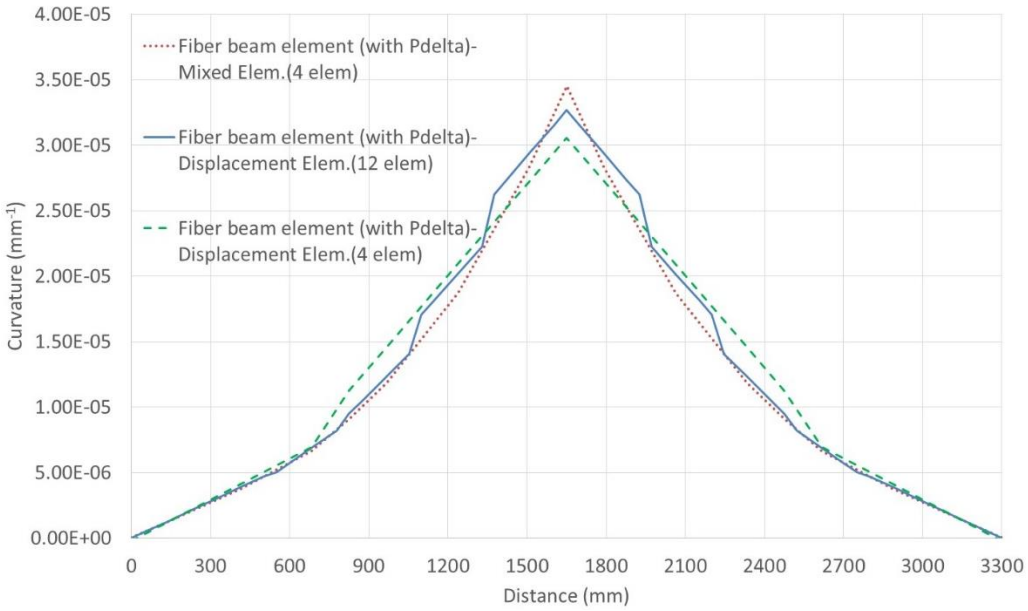

Figure (10): Comparison between the Curvature at Maximum Lateral Load for the New and Original Fibre Beam Elements

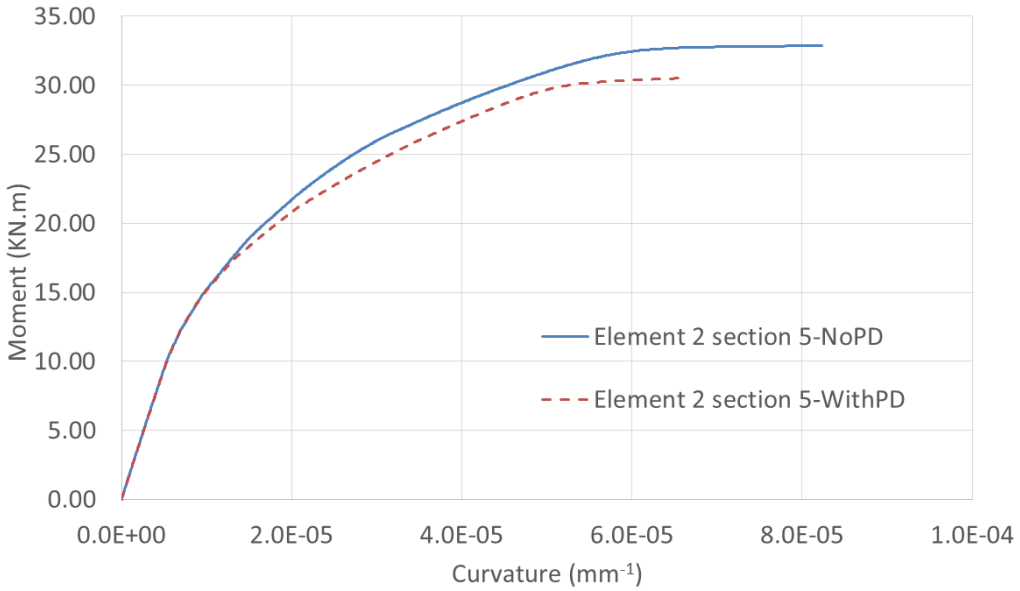

Figure (11): Moment curvature relationship for element 2-section 5 of Barrera et al. Specimen

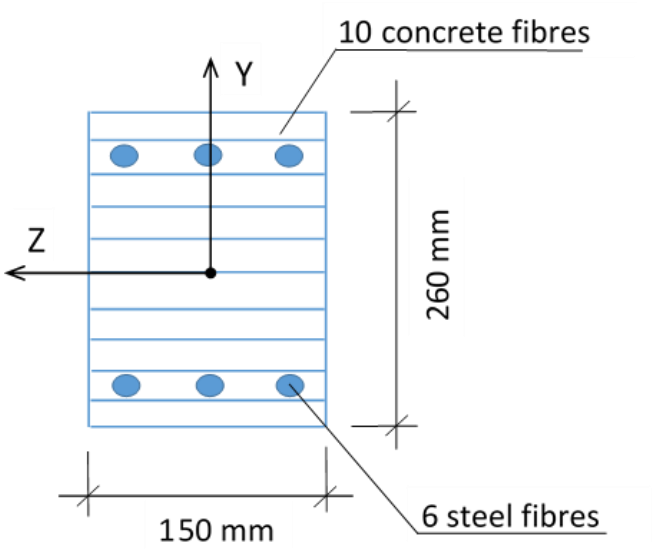

Figure (12): Fibre beam element cross section mesh for specimens NF00L05V2S100 and HF60L05V1S50

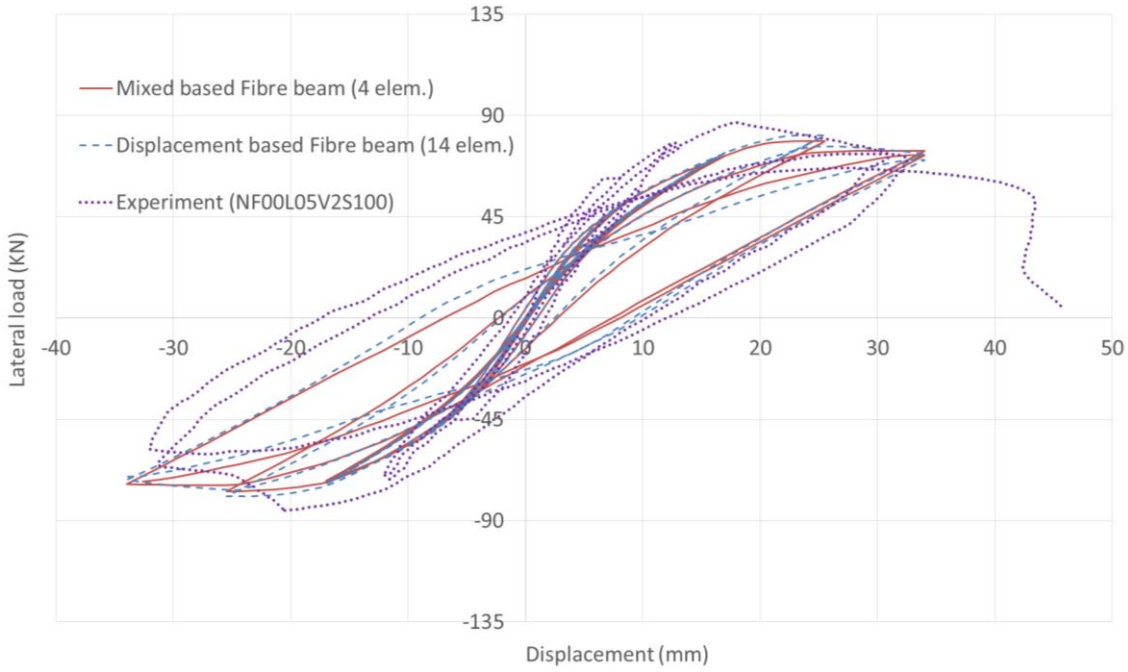

Figure (13): Analytical and Experimental Load Displacement Curve for Column NF00L05V2S100

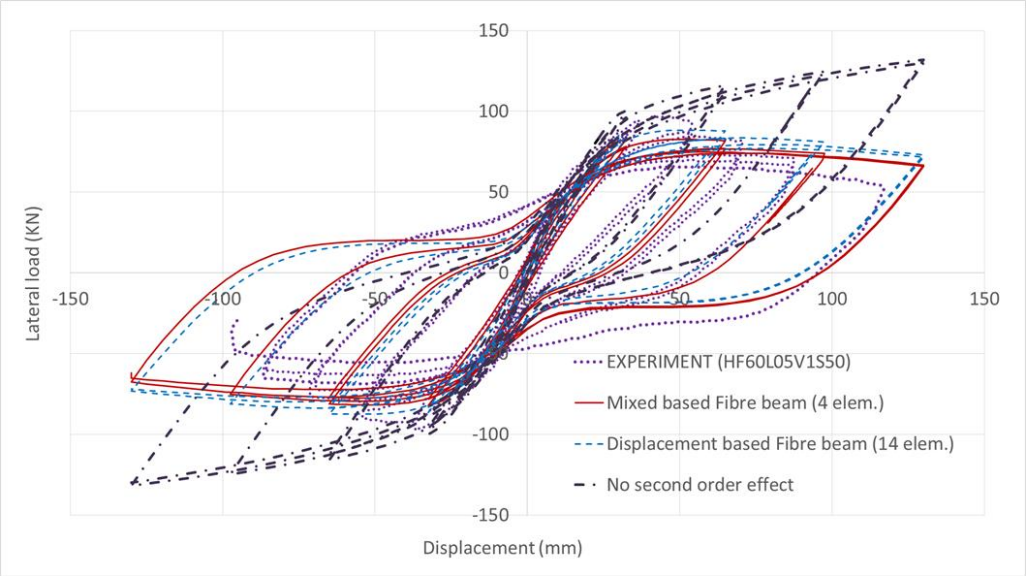

Figure (14): Analytical and Experimental Load Displacement Curve for Column HF60L05V1S50

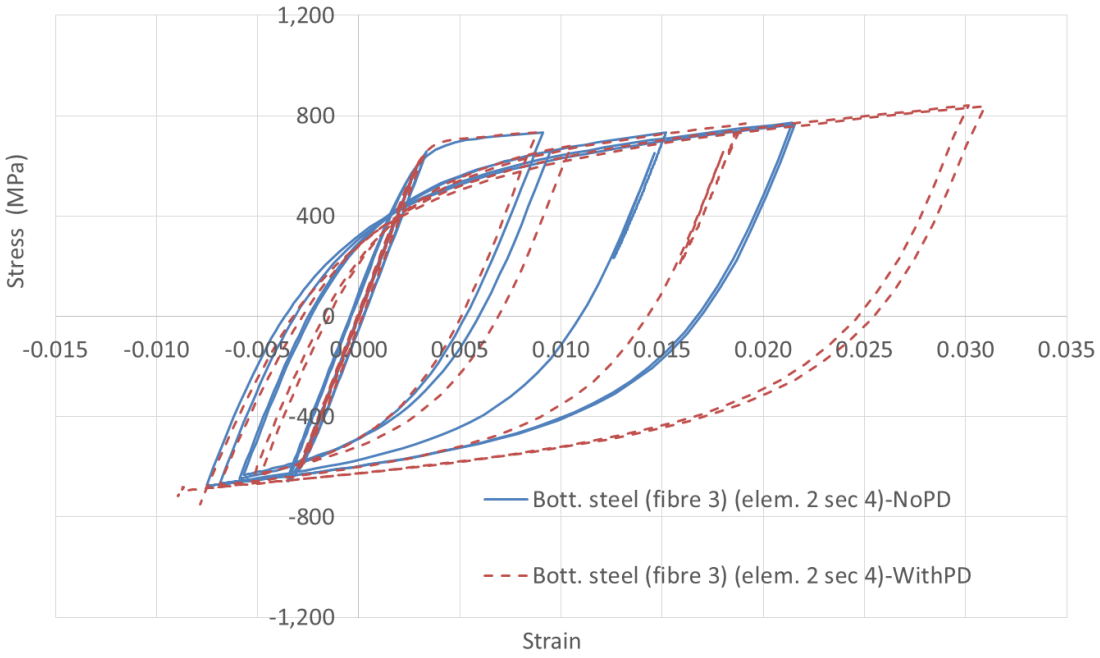

Figure (15): Comparison between the Stress-Strain Curves of Bottom Steel Fibre 3 for Element 2 at Sec. 4 using the Mixed Element with and without the Second Order Effect (sample HF60L05V1S50)

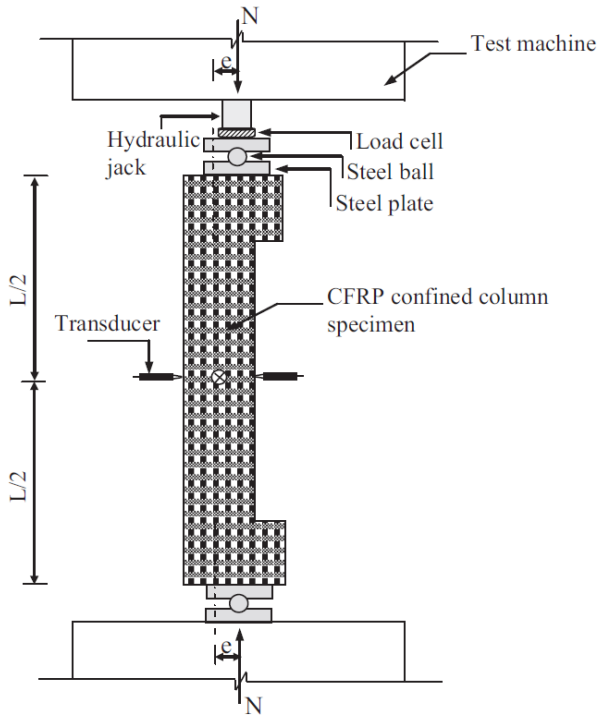

Figure (16): Experiment setup of Dundar et al. Specimen [22]

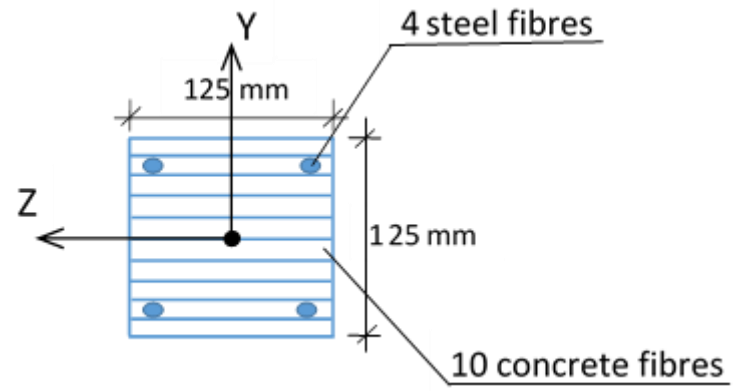

Figure (17): Fibre beam element cross section mesh for intermediate section of specimens C2-II-SF and C2-II

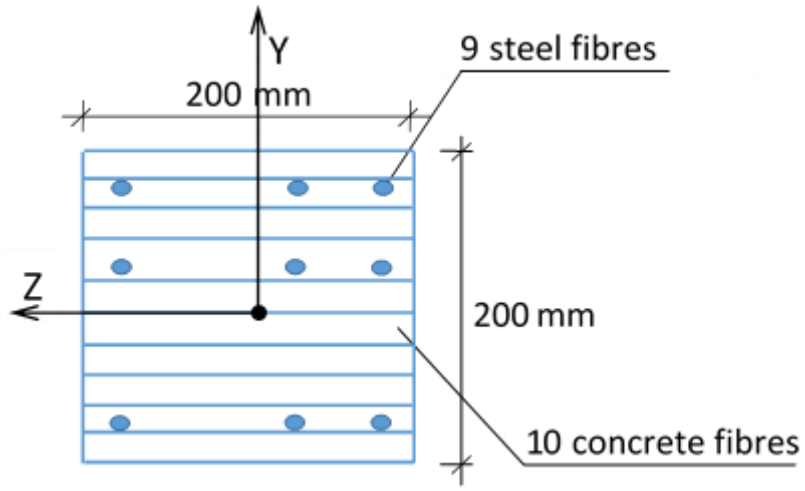

Figure (18): Fibre beam element cross section mesh for end sections of specimens C2-II-SF and C2-II

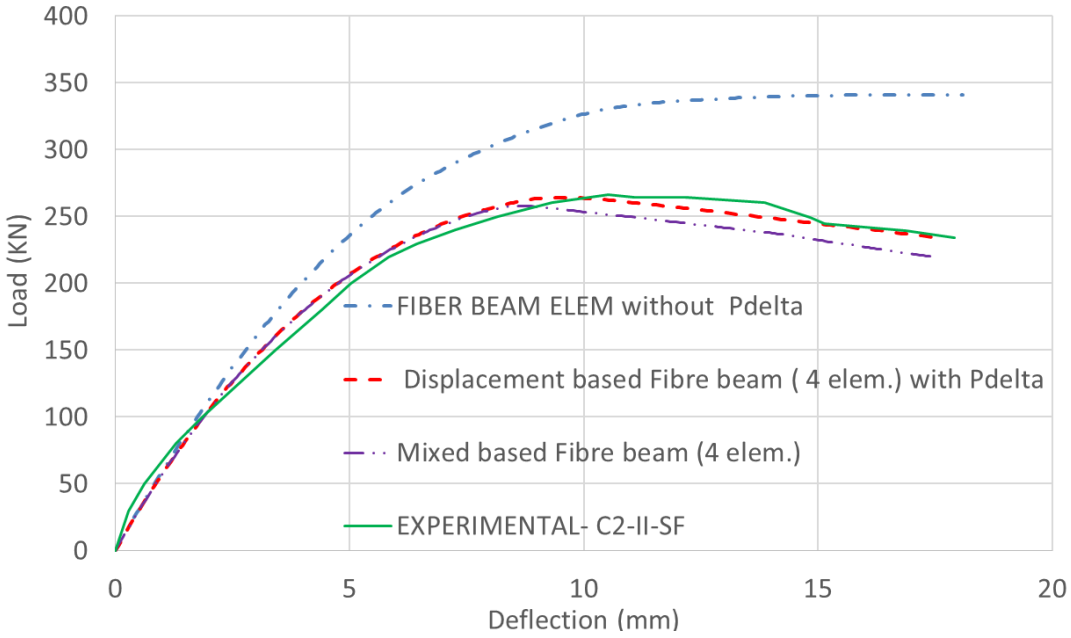

Figure (19): Analytical and Experimental Load-Deflection Curve for Column C2-II-SF

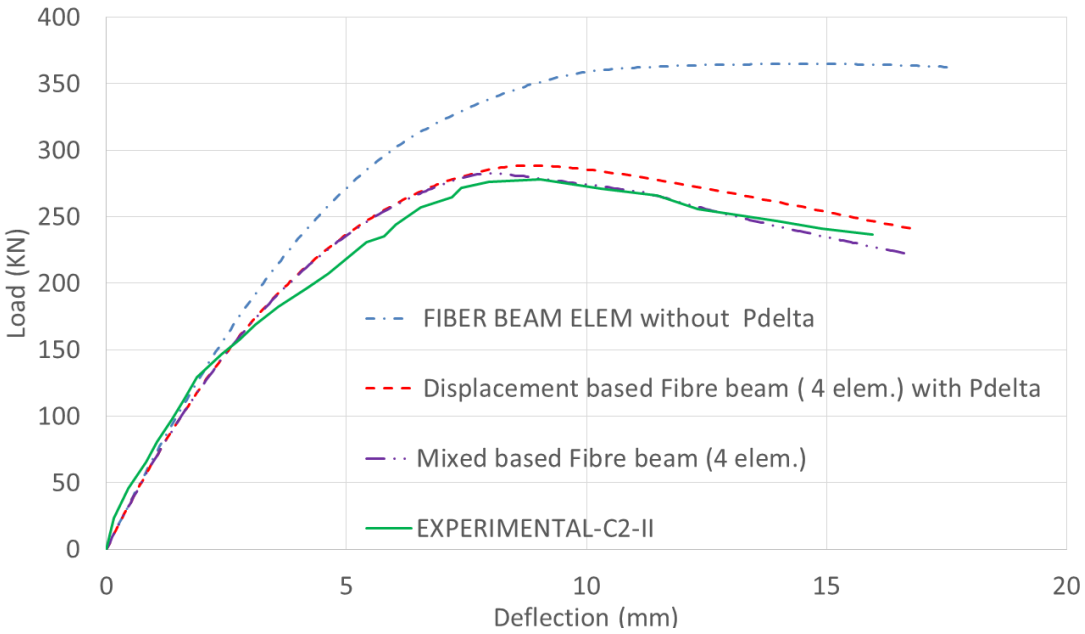

Figure (20): Analytical and Experimental Load-Deflection curve for column C2-II

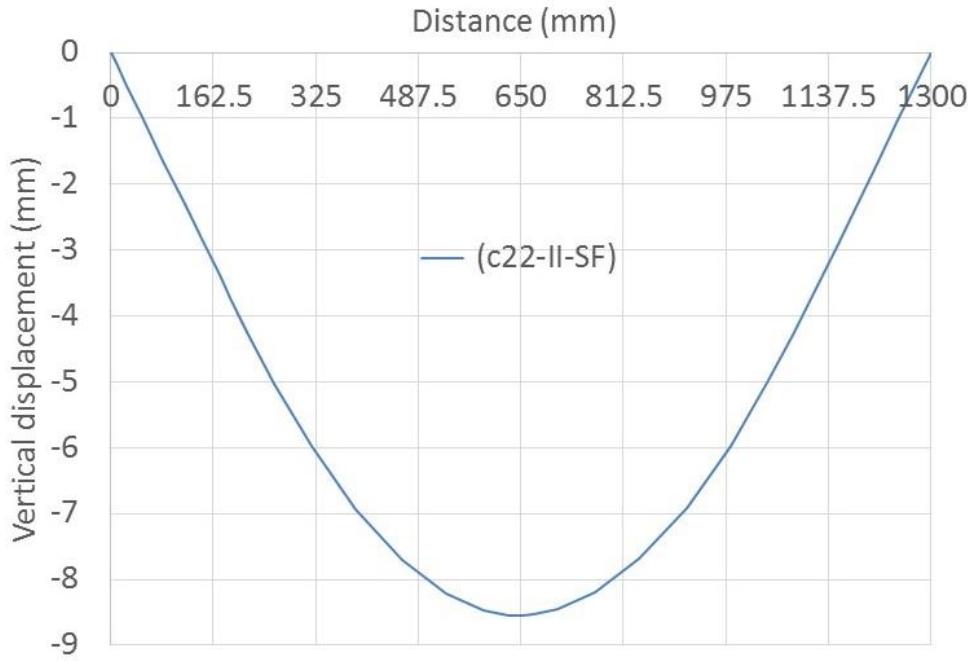

Figure (21): Vertical Displacement along the Column Length at Maximum Load for column C2-II-SF using the Mixed Fibre Beam Element

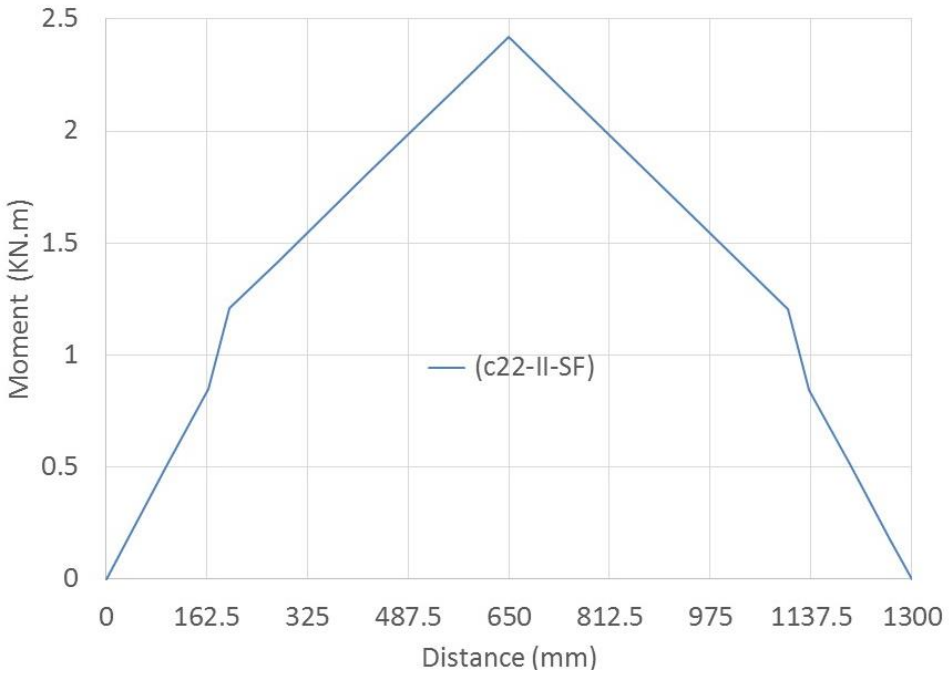

Figure (22): Moment along the Column Length at Maximum Load for Column C2-II-SF using the Mixed Fibre Beam Element